Check for updates

VIP Heterogeneous Catalysis Very Important Paper

Deutsche Ausgabe: DOI: 10.1002/ange.201810538
Internationale Ausgabe: DOI: 10.1002/anie.201810538

The p-Orbital Delocalization of Main-Group Metals to Boost CO_2 Electroreduction

Sisi He[+], Fenglou Ni[+], Yujin Ji[+], Lie Wang, Yunzhou Wen, Haipeng Bai, Gejun Liu, Ye Zhang, Youyong Li, Bo Zhang,* and Huisheng Peng**

Abstract: *Enhancing the p-orbital delocalization of a Bi catalyst (termed as POD-Bi) via layer coupling of the short inter-layer Bi–Bi bond facilitates the adsorption of intermediate *OCHO of CO_2 and thus boosts the CO_2 reduction reaction (CO_2RR) rate to formate. X-ray absorption fine spectroscopy shows that the POD-Bi catalyst has a shortened inter-layer bond after the catalysts are electrochemically reduced in situ from original BiOCl nanosheets. The catalyst on a glassy carbon electrode exhibits a record current density of 57 mA cm^{-2} (twice the state-of-the-art catalyst) at −1.16 V vs. RHE with an excellent formate Faradic efficiency (FE) of 95 %. The catalyst has a record half-cell formate power conversion efficiency of 79 % at a current density of 100 mA cm^{-2} with 93 % formate FE when applied in a flow-cell system. The highest rate of the CO_2RR production reported (391 mg h^{-1} cm^{2}) was achieved at a current density of 500 mA cm^{-2} with formate FE of 91 % at high CO_2 pressure.*

Electrochemical reduction of CO_2 to useful fuels and chemicals offers a means to store renewable electricity at high volume and mass density with the ability to utilize existing infrastructure for transportation and distribution.[1] As an important product of CO_2 reduction reaction (CO_2RR), formate has a high product value per electron ($\$16.1\times10^{-3}$/electron).[2] Moreover, formate has various useful industrial applications such as a raw material for the pharmaceutical synthesis, a promising chemical for hydrogen storage, an anode fuel for fuel cells and a raw chemical to be converted into syngas.[3] Various metal catalysts have been evaluated with a wide range of Faradic efficiency (FE) and current density for formate production. Abundant main-group metals such as Bi, Sn, and Pb have been found to be good catalysts to produce formate with FE greater than 90 % in CO_2-saturated aqueous HCO_3^- solution.[4] Unfortunately, the reduction activity has been far too low for practical applications, that is, the current densities are generally below 10 mA cm^{-2} and production rates are below 30 mg h^{-1} cm^{2},[5] which greatly increases electrolyzer capital cost and makes production uneconomical.[2] Furthermore, the power conversion efficiency (chemical energy stored in the desired products versus input electric energy) is also a vital figure of merit, which is mainly limited by the overpotentials of CO_2 to formate reaction and anodic reaction (water oxidation). Recent technoeconomic analyses have identified formate as a profitable product only when current densities reach at least 200 mA cm^{-2}, FEs greater than 90 %, and power conversion efficiencies more than 50 %.[2,6] Improvement in simultaneously achieving high current densities, high production rates, high selectivity, and satisfactory power conversion efficiencies are required to make formate economically viable and increase its demand, but unfortunately not yet achieved.[2,3a]

Transition metals have been widely applied for the electroreduction of CO_2 due to the availability of their versatile d-orbital electron states to participate in adsorption as described in d-band theory.[7] Numerous strategies, such as quantum size tuning of nanoparticles,[8] heteroatom doping,[9,10] and reactive surface modulation,[11,12] have been explored to modulate their versatile d-orbital electron states to obtain a higher activity.[7] For instance, after introducing Se and S into Mo to synthetize a MoSeS alloy, the shortened Mo–S and lengthened Mo–Se bonds allow for the modulation of the d-band electronic structure of Mo atoms. The current density towards CO production during CO_2RR was increased from 16 to 43 mA cm^{-2}.[9c] However, most transitional metals fail to produce formate effectively due to the intrinsic stronger binding of the *COOH intermediate, inhibiting further reduction.[13]

In contrast to the easily tunable and delocalized electronic structure of d-orbitals in transition metals, main-group metals exhibit localized p-orbital electron states.[14] It has been hypothesized that delocalized d electrons are the origin of the high catalytic activity of transition metals.[7,8b] We posit that modulating the electron density of localized p-orbitals in main-group metals into delocalized states and thus endowing versatile electronic structures, may impart p-orbital character similar to transition metals, and thus enhance the reduction activity to produce formate.

Herein, using density functional theory (DFT) simulation, we discovered that the delocalization degree of the Bi-p orbital can be tuned by compressing the inter-layer Bi–Bi bond length. Furthermore, the Bi-p orbital delocalization

[*] S. He,[+] F. Ni,[+] L. Wang, Y. Wen, H. Bai, G. Liu, Y. Zhang, B. Zhang, H. Peng
State Key Laboratory of Molecular Engineering of Polymers
Department of Macromolecular Science and
Laboratory of Advanced Materials, Fudan University
Shanghai 200438 (China)
E-mail: bozhang@fudan.edu.cn
penghs@fudan.edu.cn
Y. Ji,[+] Y. Li
Institute of Functional Nano & Soft Materials (FUNSOM), Jiangsu Key Laboratory for Carbon-Based Functional Materials & Devices
Soochow University, Suzhou, Jiangsu 215123 (China)
E-mail: yyli@suda.edu.cn
[+] These authors contributed equally to this work.
Supporting information and the ORCID identification number(s) for the author(s) of this article can be found under: https://doi.org/10.1002/anie.201810538.

© 2018 Wiley-VCH Verlag GmbH & Co. KGaA, Weinheim

facilitates the adsorption of intermediate *OCHO of CO_2, thus improving the electrocatalytic activity. Experimentally, we synthesized p-orbital localized Bi (POD-Bi) catalysts that exhibit a compressed inter-layer bond length by electrochemically reducing BiOCl nanosheets. The POD-Bi catalyst under high pressure reached a record partial current density of 500 mA cm^{-2} and a record production rate of 391 mg h^{-1} cm^2 with a FE of 91%, two times higher than the previous reports (Supporting Information, Table S3).

We first sought to modulate the p-orbital of Bi by tuning the bond length of inter-layer Bi and then investigated this effect on the thermodynamic energetics of CO_2RR. As shown in Figure 1a, conventional Bi metal exhibits a layered structure with an intra-layer Bi–Bi bond length of 3.07 Å and an inter-layer Bi–Bi bond length of 3.53 Å. It has been reported that the energetically favored reaction step after the first protonation of CO_2 is the formation of *OCHO immediate with a Bi–O bond on the Bi(012) surface.[15] Herein, we modeled a series of Bi (012) surfaces with different inter-layer Bi–Bi bond lengths to tune the Bi p-orbital delocalization and investigate its effects on CO_2RR activity. Results show that the delocalized degrees of Bi electron states increase with the decreasing inter-layer Bi–Bi bond length. The electronic distribution of inter-layer Bi atoms in real space will couple with each other due to the compressed structure, which is responsible for the delocalization electrons across Bi-p orbitals (Figure 1b). Furthermore, Figure 1c and d reveal that the projected density of state (PDOS) of Bi-p electrons tend to delocalize into deeper energy levels and have a linear relationship with the adsorption free energy G(*OCHO). The p-orbital delocalization of Bi atoms leads to greater orbital hybridization between the surface Bi atom and an adsorbed *OCHO, clearly enhancing the interaction energies of *OCHO. Meanwhile, more electronic states through the Fermi level will facilitate the electron transfer ability and enhance the reduction of CO_2 on the electrode surface. From DFT simulations, the Bi with short inter-layer bond length tends to exhibit a better electrocatalytic performance because of delocalized p-electrons and electronic conductance through the inter-layer coupling.

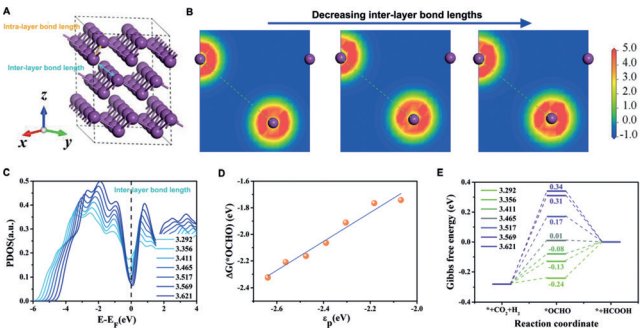

Figure 1. DFT calculations of electrocatalytic CO_2 into formate on Bi by tuning the Bi–Bi bond length. A) The crystal structure of bulk Bi. B) The electronic distribution between two neighboring inter-layer Bi atoms. C) PDOS of the external p orbital of the Bi atom. D) The relationship between p-band center and adsorption free energy of *OCHO. E) The calculated free energy diagrams of electrocatalytic CO_2 into formate without considering the effect of electrode potential ($U = 0$ V).

It was found that the adsorption energy of the intermediate *OCHO increased with the decrease of inter-layer Bi–Bi bond length. This leads to a decreased activation barrier in the first protonation of CO_2, and correspondingly enhance the performance of CO_2RR towards formate. Interestingly, when the inter-layer Bi–Bi bond length decreases to 3.36 Å, the overpotential of *OCHO is predicted to be near-zero (0.01 eV), as shown in Figure 1e. These theoretical simulations suggest that optimizing the degree of Bi p-orbital delocalization via inter-layer compression may provide an enhanced electrocatalytic performance.

Inspired by the DFT prediction of valuable p-orbital delocalization, we sought to synthesize Bi catalysts with short inter-layer bond lengths. It is impressive to find that Bi catalysts can possess short inter-layer bond lengths, when prepared via electrochemically reducing bismuth oxychloride (BiOCl) in situ. For comparison, commercial Bi was chosen as a control sample. We carried out in situ X-ray absorption fine spectroscopic (XAFS) method to analyze the electronic structure of formed Bi during in situ electrochemical reducing BiOCl. To make sure the stability of XAFS measurement during the reduction process, we conducted a chronamperometry electroreduction at −0.76 V vs. reversible hydrogen electrode (RHE) in CO_2-saturated 0.5 M $KHCO_3$ aqueous solution (see details in Methods in the Supporting Information). Figure 2a shows the Bi L_3-edge normalized absorption spectra of the BiOCl during the electrochemical reducing process, as well as commercial Bi as a comparison. During 20 min reduction reaction, a notable feature of the Bi^{3+} in the BiOCl at 13.44 keV gradually shifted to higher energy at 13.45 keV which contributed to the metallic Bi, while the spectra of commercial Bi remained almost unchanged (Supporting Information, Figure S1). The overlapped curves imply that the BiOCl was almost reduced to metallic Bi after reduction reaction. The k^2-weighted XAFS χ versus reciprocal wave vector indicated good qualities of the data (Figure 2b). The absolute of measured spectrum that is, $|\chi(R)|$, was derived from Fourier transformation by transforming the above measured spectrum to real R-space produced $\chi(R)$ (Figure 2c). The $|\chi(R)|$ exhibits the dependence of the density of neighboring atoms on real distance (R).[16] By fitting the measured spectrum with the window from 1 to 4 Å, we obtained the bond lengths of POD-Bi and commercial Bi. The measured bond lengths of commercial Bi are 3.1 Å and 3.7 Å, and the POD-Bi are 3.1 Å and 3.4 Å, which correspond to intra- and inter-layer spacings, respectively (Figure 2d). We further conducted X-ray diffraction patterns, and the reduced Bi possessed obvious characteristic peaks at 27.2°, 38.0°, 39.6°, and 48.8°, corresponding to the (012), (104), (110), and (202) facets of metallic Bi, respectively (Supporting Information, Figure S2), which is almost the same to the control sample of commercial Bi sample (Supporting Information, Figure S3). However, the peak showed an obviously shift with the control commercial Bi sample with a higher degree, which accordingly indicates a shorter inter-layer bond length (Supporting Information, Figure S4).[17] These results point towards that a POD-Bi

 © 2018 Wiley-VCH Verlag GmbH & Co. KGaA, Weinheim

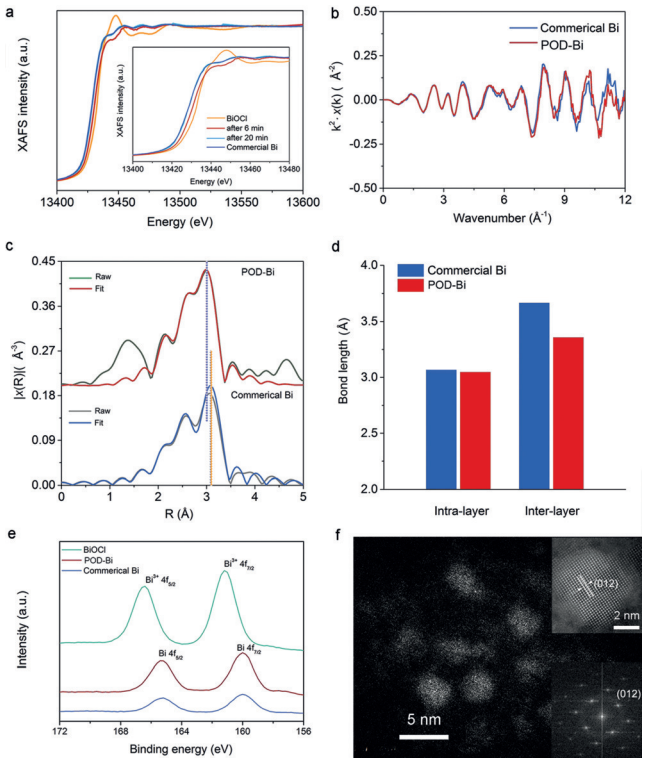

Figure 2. Characterization of POD-Bi and commercial Bi. a) Bi L_3-edge XAFS spectra of BiOCl after reduction at −0.76 V vs. RHE in CO_2-saturated electrolyte with the comparison of commercial Bi. b) The k^2-weighted XAFS $\chi(k)$ of POD-Bi and commercial Bi. c) Bi L_3-edge extended XAFS spectra of POD-Bi and commercial Bi. d) Bond lengths of the POD-Bi and commercial Bi. e) Bi 4f XPS spectra of BiOCl, POD-Bi and commercial Bi. f) Scanning transmission electron microscopy image of POD-Bi (inset, corresponding magnified image showing the lattice and selected area electron diffraction pattern).

catalyst possesses a shorter inter-layer bond length than the conventional Bi.

We also conducted X-ray photoelectron spectroscopy (XPS) measurements to further investigate the chemical nature of the reduced Bi catalyst. In the high-resolution XPS spectra of Bi 4f shown in Figure 2e and the Supporting Information, Figure S5, two obvious peaks at 161.2 and 166.4 eV that correspond to Bi^{3+} were found.[5c,18] After reduction, these two peaks disappeared and another two predominant peaks at 160.0 eV and 165.3 eV can be observed which ascribed to metallic Bi^0.[19] We then used scanning transmission electron microscopy to track the morphology and growth of the POD-Bi catalyst after the in situ reduction. The as-prepared BiOCl were single-crystalline nanosheets with a uniform width of about 500 nm and thickness of about 10 nm (Supporting Information, Figure S6). The nanosheets were electrochemically reduced under cyclic voltammetry method in CO_2-saturated 0.5 M $KHCO_3$ aqueous solution (Supporting Information, Figure S7). With potentials scanning from −0.2 to −1.4 V vs. RHE, an obvious cathodic peak at −1.1 V indicates that BiOCl was reduced. After two cycles, the cathodic peak disappeared, suggesting that BiOCl was thoroughly reduced to metallic state. After in situ electrochemical reduction, the original nanosheets turned into nanoparticles (Supporting Information, Figure S8). Furthermore, high-resolution transmission electron microscopy showed that the resultant reduced Bi was consisted of fine nanocrystals. The nanoparticle diameter was found to be uniform (ca. 5 nm; Figure 2 f). It can be concluded that during in situ electrochemical reduction process, BiOCl was reduced to metallic Bi but with compressed inter-layer Bi–Bi bond length. According to the DFT simulation results, p-orbital delocalization, that is, POD-Bi, is formed.

To verify the DFT prediction of the effect of p-orbital delocalization on CO_2RR performance, we conducted chronopotentiometry experiments on POD-Bi and commercial Bi on glassy carbon electrodes (GCEs) at the range of −0.86 to −1.36 V vs. RHE for 3600 s at each applied potential in CO_2-saturated 0.5 M $KHCO_3$ aqueous electrolytes in H-cell system, respectively. A maximal formate FE ($FE_{formate}$) of 95 % was obtained on POD-Bi at the potential of −1.16 V vs. RHE. The corresponding partial current density reached 57 mA cm^{-2}, which is almost four times higher than that of commercial Bi (15 mA cm^{-2}) under the same condition. Moreover, the maximal $FE_{formate}$ can be well maintained at a large range of −0.86 to −1.36 V vs. RHE (Figure 3 a), with few side-products

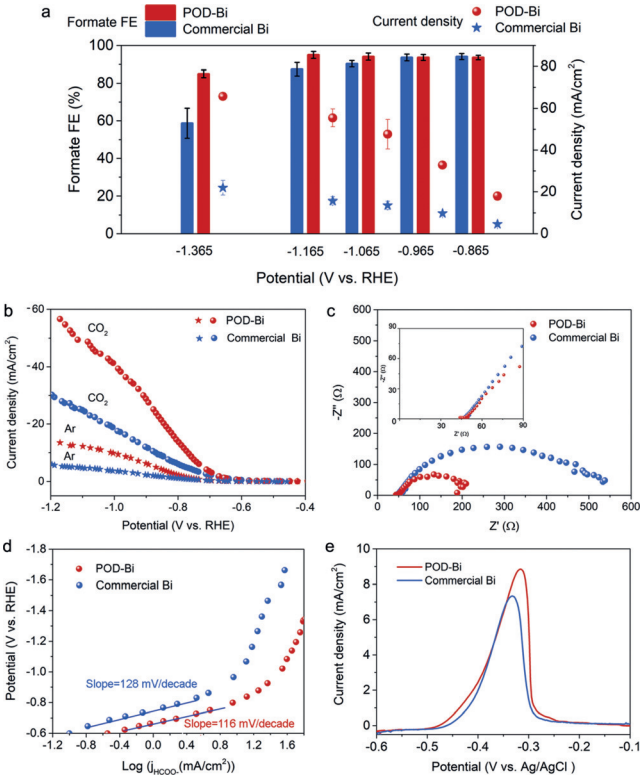

Figure 3. CO_2 reduction performance of POD-Bi and commercial Bi. a) Potential dependence of FEs and current densities for electrochemical reduction of CO_2 of POD-Bi and commercial Bi on GCE in CO_2-saturated 0.5 M $KHCO_3$ aqueous electrolyte. b) The electrochemical reduction of CO_2 polarization curves of POD-Bi and commercial Bi in CO_2- and Ar-saturated 0.5 M $KHCO_3$ aqueous electrolyte. c) Nyquist plots for POD-Bi and commercial Bi at −1.16 V vs. RHE (inset, corresponding magnified image). d) Partial current density Tafel plots for POD-Bi and commercial Bi. e) Linear sweep voltammetry curves of POD-Bi and commercial Bi after stripping from underpotential deposited Pb.

© 2018 Wiley-VCH Verlag GmbH & Co. KGaA, Weinheim

of CO (FE = 2–3 %) and H_2 (FE = 2–5 %; Supporting Information, Figure S9). When the potential was further increased, the $FE_{formate}$ started to decrease due to the favorable H_2 evolution at higher potentials, but the partial current density was still much higher than those for the reported metal catalysts in aqueous solution. However, the commercial Bi exhibited only a peak $FE_{formate}$ at the potential of −1.06 V and decreased at both higher and lower potentials (Supporting Information, Figure S10). To evaluate the effect of Cl element on BiOCl precursor, we conducted the electrocatalytic performance of POD-Bi in fresh electrolytes, and found that the performance was almost the same as before, indicating that the leached Cl ions had no influence on the performance. Generally, the POD-Bi yielded a higher partial current density with a higher selectivity for formate than that of commercial Bi.

To further investigate the CO_2RR performance, we conducted cyclic voltammograms of catalysts in CO_2-saturated 0.5 M $KHCO_3$ aqueous electrolyte and compared with the results obtained in the blank Ar-saturated 0.5 M $KHCO_3$ aqueous electrolyte in H-cell system. The linear sweep voltammetry results in Figure 3b showed that a cathodic current of POD-Bi quickly increased at potentials more negative than −0.54 V vs. RHE in both electrolytes. The onset potential of POD-Bi was more positive than that of the commercial Bi. The current densities of catalysts were obviously increased in CO_2-saturated electrolyte in comparison with those in Ar-saturated electrolyte, and a larger increase for POD-Bi was also observed compared with the commercial Bi, indicating that the POD-Bi exhibited higher CO_2 reduction current. The above results demonstrate that POD-Bi exhibits higher reduction rate, lower overpotential and higher catalytic activity.

To better understand the charge transfer at the solid/electrolyte interface of these two catalysts, we applied electrochemical impendence spectroscopy (EIS) to investigate them on GCEs at −1.16 V vs. RHE. The obtained Nyquist plots showed that the high-frequency intercepts on the real axis of two catalysts (R_s) were almost the same, suggesting the similar series resistances which included the resistances of catalysts and GCE and the contact resistance (Figure 3c). The charge transfer resistance (R_{ct}) was directly proportional to the diameter of the semicircle in the spectra, and it represents the ease of charge exchange between the catalyst and reactants in the electrolyte. Obviously, the R_{ct} of the reduced Bi was 171 Ω, which is much lower than that of the commercial Bi (471 Ω), indicating that POD-Bi has higher catalytic activity than the commercial one.[20]

To further explore the experimental mechanistic pathways for the CO_2RR in the POD-Bi catalyst, the Tafel plots were investigated (Figure 3d). At a lower current density, the slope values of POD-Bi and commercial Bi are 116 and 128 mV/decade, respectively. The similar values of the two catalysts are close to 118 mV/decade, pointing towards that an initial electron transfer rate is the determining step for both catalysts,[21] consistent with the DFT results. The fast electron transfer to CO_2 can form a short-lived surface to adsorb $CO_2^{\bullet-}$ intermediate. Moreover, the Tafel slope of POD-Bi is smaller than that of commercial Bi, showing an increased CO_2 reduction kinetic.[22]

To explore the intrinsic performance of these two catalysts and to eliminate the effect of crystal size and real surface area on the CO_2RR performance, we measured the electrochemical surface area (ECSA) by Pb underpotential deposition (UPD) method (Figure 3e).[23] These two catalysts were coated on GCEs, and the obtained Pb-stripping curves demonstrated an obvious peak at −0.32 V vs. Ag/AgCl, which represents Pb monolayer deposition on Bi catalyst surface. After calculation, from the consumed charge, the ECSAs of POD-Bi and commercial Bi were 51.6 and 38.7 $cm^2 mg^{-1}$, respectively. To further confirm these results, we also conducted Cu UPD, which was in good agreement with that obtained by Pb UPD (Supporting Information, Figure S11).[24] It implied that the ECSA of POD-Bi was 1.3 times larger than that of the commercial Bi, which may be due to the smaller particle size of POD-Bi. When the current densities were re-normalized by the ECSA, the partial current density of POD-Bi at −1.16 V vs. RHE was still 3.2 times higher than that of commercial Bi, indicating a much higher intrinsic catalytic activity of POD-Bi. The experimental activity of these shortened inter-layer Bi catalysts suggest that p-orbital delocalization can facilitate the production of $HCOO^-$, which is good consistent with our DFT calculation results.

To further increase the catalytic current density and production rate towards industrial applications, we explored methods including a flow-cell reactor and a stainless steel high-pressure reactor with our catalysts.[25] In a flow-cell configuration, by using the gas diffusion electrodes, the mass transport limitation was minimized and the rate of electrochemical reduction for CO_2 can be greatly increased. We first measured R_s via EIS (Supporting Information, Figure S12) and obtained 95 % *iR* corrected polarization curves (Supporting Information, Figure S13). The current density of POD-Bi reached 200 mA cm^{-2} at −0.61 V vs. RHE, much higher than the reported best (Supporting Information, Figure S14 and S15 and Table S2). Moreover, FE for $HCOO^-$ production was still above 93 % at 200 mA cm^{-2}, demonstrating a high catalytic activity and selectivity of POD-Bi even at such a high current density. Furthermore, the half-cell formate power conversion efficiency of POD-Bi reached 79 % at 100 mA cm^{-2} (Supporting Information, Table S2). Furthermore, we explored another strategy to increase the current density by increasing the dissolved amount of CO_2 in the electrolyte under high CO_2 pressure. We also obtained 95 % *iR* corrected chronopotential curves on GCE in 0.5 M $KHCO_3$ solution with the applied pressure of 5.6 MPa (Supporting Information, Figure S16; Figure 4a). The current density further gradually increased to 500 mA cm^{-2}. At the same time, the selectivity for $HCOO^-$ production was still more than 90 % (Figure 4b). The production rate reached a record value of 391 mg $h^{-1} cm^2$ at the so high current density with a faradaic efficiency of 91 % (Figure 4b), which is more than 2 times higher than the state-of-the-art synthesized catalysts (Supporting Information, Table S3).

In conclusion, we have developed a powerful strategy to achieve a highly efficient Bi catalyst for electrochemical CO_2

 © 2018 Wiley-VCH Verlag GmbH & Co. KGaA, Weinheim

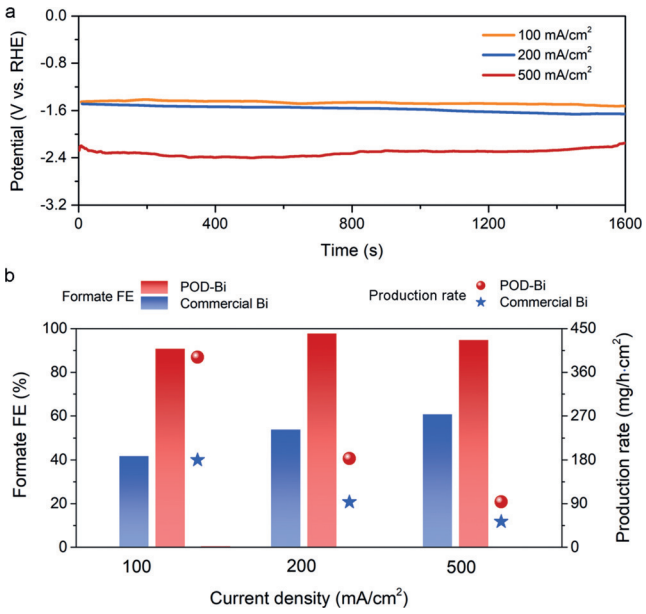

Figure 4. High current densities of POD-Bi under high pressure. a) Potential dependence on time during reduction at 100, 200 and 500 mA cm^{-2} in 0.5 M $KHCO_3$ aqueous electrolyte on the GCE at 5.6 MPa CO_2 pressure. b) Corresponding formate FEs and production rates of POD-Bi and commercial Bi under reduction at 100, 200, and 500 mA cm^{-2}.

reduction by optimizing inter-layer bond length to tune the electron density of localized p-orbital in a main-group metal into its delocalized states, combining the DFT simulation and experimental verification. This work provides a new pathway for further advances to the development of main-group catalysts along this crucial front via p-orbital delocalization.

Acknowledgements

This work was supported by Ministry of Science and Technology (2016YFA0203302), National Natural Science Foundation of China (grants 21503079, 21634003, 51573027, 51673043, 21875042, and 21604012), Science and Technology Commission of Shanghai Municipality (grants 18QA1400800, 16JC1400702, 15XD1500400, and 15JC1490200), SHMEC (2017-01-07-00-07-E00062) and the Shanghai youth talent support program. The transmission microscopy study in this work was supported by the Frontier Research Center for Materials Structure, School of Materials Science and Engineering of Shanghai Jiao Tong University.

Conflict of interest

The authors declare no conflict of interest.

Keywords: bismuth · CO_2 electroreduction · delocalization · formate · heterogeneous catalysis

How to cite: *Angew. Chem. Int. Ed.* **2018**, *57*, 16114–16119
Angew. Chem. **2018**, *130*, 16346–16351

[1] a) D. Deng, K. S. Novoselov, Q. Fu, N. Zheng, Z. Tian, X. Bao, *Nat. Nanotechnol.* **2018**, *11*, 218–230; b) R. G. Mariano, K. Mckelvey, H. S. White, M. W. Kanan, *Science* **2017**, *358*, 1187–1192; c) S. Lin, C. S. Diercks, Y. Zhang, N. Kornienko, E. M. Nichols, Y. Zhao, A. R. Paris, D. Kim, P. Yang, O. M. Yaghi, C. J. Chang, *Science* **2015**, *349*, 1208–1213.

[2] M. Jouny, W. Luc, F. Jiao, *Ind. Eng. Chem. Res.* **2018**, *57*, 2165–2177.

[3] a) A. S. Agarwal, Y. M. Zhai, D. Hill, N. Sridhar, *ChemSusChem* **2011**, *4*, 1301–1310; b) P. Sponholz, D. Mellmann, H. Junge, M. Beller, *ChemSusChem* **2013**, *6*, 1172–1176.

[4] a) H. Zhang, Y. Ma, F. J. Quan, J. J. Huang, F. L. Jia, L. Z. Zhang, *Electrochem. Commun.* **2014**, *46*, 63–66; b) Y. Chen, M. W. Kanan, *J. Am. Chem. Soc.* **2012**, *134*, 1986–1989; c) H. L. Chang, M. W. Kanan, *ACS Catal.* **2015**, *5*, 465–469.

[5] a) S. Zhang, P. Kang, T. J. Meyer, *J. Am. Chem. Soc.* **2014**, *136*, 1734–1737; b) W. X. Lv, J. Zhou, J. Bei, R. Zhang, L. Wang, Q. Xu, W. Wang, *Appl. Surf. Sci.* **2017**, *393*, 191–196; c) H. X. Zhong, Y. L. Qiu, T. T. Zhang, X. F. Li, H. M. Zhang, X. B. Chen, *J. Mater. Chem. A* **2016**, *4*, 13746–13753.

[6] O. S. Bushuyev, P. D. Luna, C. T. Dinh, L. Tao, G. Saur, J. Lagemaat, S. O. Kelley, E. H. Sargent, *Joule* **2017**, https://doi.org/10.1016/j.joule.2017.09.003.

[7] M. Asadi, B. Kumar, A. Behranginia, B. A. Rosen, A. Baskin, N. Repnin, D. Pisasale, P. Phillips, W. Zhu, R. Haasch, R. F. Klie, P. Král, J. Abiade, A. Salehi-Khojin, *Nat. Commun.* **2014**, *5*, 4470.

[8] a) W. L. Zhu, R. Michalsky, Ö. Metin, H. Lv, S. Guo, C. J. Wright, X. Sun, A. A. Peterson, S. Sun, *J. Am. Chem. Soc.* **2013**, *135*, 16833–16836; b) D. F. Gao, H. Zhou, J. Wang, S. Miao, F. Yang, G. Wang, J. Wang, X. Bao, *J. Am. Chem. Soc.* **2015**, *137*, 4288–4291.

[9] a) S. Rasul, D. H. Anjum, A. Jedidi, Y. Minenkov, L. Cavallo, K. Takanabe, *Angew. Chem. Int. Ed.* **2015**, *54*, 2146–2150; *Angew. Chem.* **2015**, *127*, 2174–2178; b) D. Kim, J. Resasco, Y. Yu, A. M. Asiri, P. D. Yang, *Nat. Commun.* **2014**, *5*, 4948; c) J. Xu, X. Li, W. Liu, Y. Sun, Z. Ju, T. Yao, C. Wang, H. Ju, J. Zhu, S. Wei, Y. Xie, *Angew. Chem. Int. Ed.* **2017**, *56*, 9121–9125; *Angew. Chem.* **2017**, *129*, 9249–9253.

[10] S. Dou, L. Tao, R. L. Wang, S. El Hankari, R. Chen, S. Y. Wang, *Adv. Mater.* **2018**, *30*, 1705850.

[11] S. Dou, X. Wang, S. Y. Wang, *Small Methods* **2018**, *2*, 1800211.

[12] a) K. Jiang, R. B. Sandberg, A. J. Akey, X. Liu, D. C. Bell, J. K. Nørskov, K. Chan, H. Wang, *Nat. Catal.* **2018**, *1*, 111–119; b) P. De Luna, R. Quintero-Bermudez, C.-T. Dinh, M. B. Ross, O. S. Bushuyev, P. Todorović, T. Regier, S. O. Kelley, P. Yang, E. H. Sargent, *Nat. Catal.* **2018**, *1*, 103–110.

[13] a) Q. Lu, J. Rosen, Y. Zhou, G. S. Hutchings, Y. C. Kimmel, J. G. Chen, F. Jiao, *Nat. Commun.* **2014**, *5*, 3242; b) R. Kas, R. Kortlever, A. Milbrat, M. T. M. Koper, G. Mul, J. Baltrusaitis, *Phys. Chem. Chem. Phys.* **2014**, *16*, 12194–12201; c) C. Hahn, D. N. Abram, H. A. Hansen, T. Hatsukade, A. Jackson, N. C. Johnson, T. R. Hellstern, K. P. Kuhl, E. R. Cave, J. T. Feastera, T. F. Jaramillo, *J. Mater. Chem. A* **2015**, *3*, 20185–20194; d) C. W. Li, M. W. Kanan, *J. Am. Chem. Soc.* **2012**, *134*, 7231–7324.

[14] D. Mukherjee, B. D. Sahoo, K. D. Joshi, S. C. Gupta, *J. Appl. Phys.* **2014**, *115*, 053702.

[15] J. H. Koh, D. H. Won, T. Eom, N.-K. Kim, K. D. Jung, H. Kim, Y. J. Hwang, B. K. Min, *ACS Catal.* **2017**, *7*, 5071–5077.

[16] H. Kim, H. S. Jeon, M. S. Jee, E. B. Nursanto, J. P. Singh, K. Chae, Y. J. Hwang, B. K. Min, *ChemSusChem* **2016**, *9*, 2097–2102.

[17] A. A. Othman, M. A. Osman, E. M. M. Ibrahim, M. A. Ali, *Ceram. Int.* **2017**, *43*, 527–533.

[18] Z. Zhang, M. Chi, G. M. Veith, P. Zhang, D. A. Lutterman, J. Rosenthal, S. H. Overbury, S. Dai, H. Zhu, *ACS Catal.* **2016**, *6*, 6255–6264.

 © 2018 Wiley-VCH Verlag GmbH & Co. KGaA, Weinheim

[19] a) Z. Jiao, Y. Zhang, S. Ouyang, H. Yu, G. Lu, J. Ye, Y. Bi, *ACS Appl. Mater. Interfaces* **2014**, *6*, 19488 – 19493; b) J. Medina-Ramos, J. L. DiMeglio, J. Rosenthal, *J. Am. Chem. Soc.* **2014**, *136*, 8361 – 8367.
[20] Q. Zhu, J. Ma, X. Kang, X. Sun, H. Liu, J. Hu, Z. Liu, B. Han, *Angew. Chem. Int. Ed.* **2016**, *55*, 9012 – 9016; *Angew. Chem.* **2016**, *128*, 9158 – 9162.
[21] a) S. Zhang, P. Kang, S. Ubnoske, M. K. Brennaman, N. Song, R. L. House, J. T. Glass, T. J. Meyer, *J. Am. Chem. Soc.* **2014**, *136*, 7845 – 7848; b) L. Zhang, Z. J. Zhao, J. L. Gong, *Angew. Chem. Int. Ed.* **2017**, *56*, 11326 – 11353; *Angew. Chem.* **2017**, *129*, 11482 – 11511.
[22] H. Mistry, A. S. Varela, C. S. Bonifacio, I. Zegkinoglou, I. Sinev, Y.-W. Choi, K. Kisslinger, E. A. Stach, J. C. Yang, P. Strasser, B. R. Cuenya, *Nat. Commun.* **2016**, *7*, 12123.
[23] a) O. A. Baturina, Q. Lu, M. A. Padilla, L. Xin, W. Li, A. Serov, K. Artyushkova, P. Atanassov, F. Xu, A. Epshteyn, T. Brintlinger, M. Schuette, G. E. Collins, *ACS Catal.* **2014**, *4*, 3682 – 3695; b) Y. Liu, S. Bliznakov, N. Dimitrov, *J. Phys. Chem. C* **2009**, *113*, 12362 – 12372.
[24] X. F. Feng, K. L. Jiang, S. S. Fan, M. W. Kanan, *J. Am. Chem. Soc.* **2015**, *137*, 4606 – 4609.
[25] a) E. Irtem, M. D. Hernández-Alonso, A. Parra, C. Fàbrega, G. Penelas-Pérez, J. R. Morante, T. Andreua, *Electrochim. Acta* **2017**, *240*, 225 – 230; b) E. Irtem, T. Andreu, A. Parra, M. D. Hernández-Alonso, S. García-Rodríguez, J. M. Riesco-García, G. Penelas-Pérez, J. R. Morante, *J. Mater. Chem. A* **2016**, *4*, 13582 – 13588.

Manuscript received: September 13, 2018
Revised manuscript received: October 11, 2018
Accepted manuscript online: October 13, 2018
Version of record online: November 8, 2018

 © 2018 Wiley-VCH Verlag GmbH & Co. KGaA, Weinheim